J. Fluid Mech. (2001), *vol.* 429, *pp.* 391–409. Printed in the United Kingdom

© 2001 Cambridge University Press

Holmboe's instability in exchange flows

By DAVID Z. ZHU[1] AND GREGORY A. LAWRENCE[2]

[1]Department of Civil & Environmental Engineering, University of Alberta, Edmonton, AB, Canada T6G 2G7
e-mail: dzhu@civil.ualberta.ca

[2]Department of Civil Engineering, University of British Columbia, Vancouver, BC, Canada V6T 1Z4
e-mail: lawrence@civil.ubc.ca

(Received 17 February 2000 and in revised form 5 September 2000)

A laboratory study of the exchange of two fluids of different density through a constant-width channel with an underwater sill has enabled us to study Holmboe's instability in greater detail than has been possible in mixing-layer experiments. The internal hydraulics of the exchange flow are such that we have been able to observe the initiation of instability, the development and behaviour of both symmetric and asymmetric Holmboe instabilities, and the suppression of the instability at bulk Richardson numbers above about 0.7. A number of stability criteria resulting from previous numerical investigations have been verified experimentally. Our laboratory measurements are consistent with theoretical predictions of wave speed and wavenumber.

1. Introduction

This study was motivated by the need to predict the exchange of fluids between two basins containing fluids of different density. Several exchange flows have attracted considerable attention because of their impact on water quality and circulation, e.g. the exchange flows through the Strait of Gibraltar (Armi & Farmer 1988), through the Bosphorous (Oguz *et al.* 1990), and through the Burlington Ship Canal (Hamblin & Lawrence 1990). Previous studies have shown that the exchange flow rate is influenced by the interfacial shear stress (Bormans & Garrett 1989; Zhu & Lawrence 2000). The interfacial shear stress is primarily determined by turbulent fluctuations, which are primarily the result of interfacial instabilities. In the present study we seek a better understanding of these interfacial instabilities in the hope that this will ultimately lead to an improvement in our ability to predict exchange flow rates and vertical mixing rates. Although our study focuses on exchange flows our results should also be relevant to salt-wedge intrusions, underflows into reservoirs, and other stratified flows (Yonemitsu *et al.* 1996; Yoshida *et al.* 1998; Dallimore, Imberger & Ishikawa 2000).

Holmboe (1962) examined the hydrodynamic stability of flows with a thin density interface relative to the shear layer thickness. Such flows often occur because of the relatively low molecular diffusivity of salt. At small Richardson numbers Holmboe (1962) predicted Kelvin–Helmholtz instability, and at higher Richardson numbers a second mode of instability (Holmboe's instability) consisting of two trains of interfacial waves travelling at the same speed, but in opposite directions with respect to the mean flow. Although there has been considerable interest in Holmboe's instability, there has been little experimental verification of its behaviour.

https://doi.org/10.1017/S002211200000286X Published online by Cambridge University Press

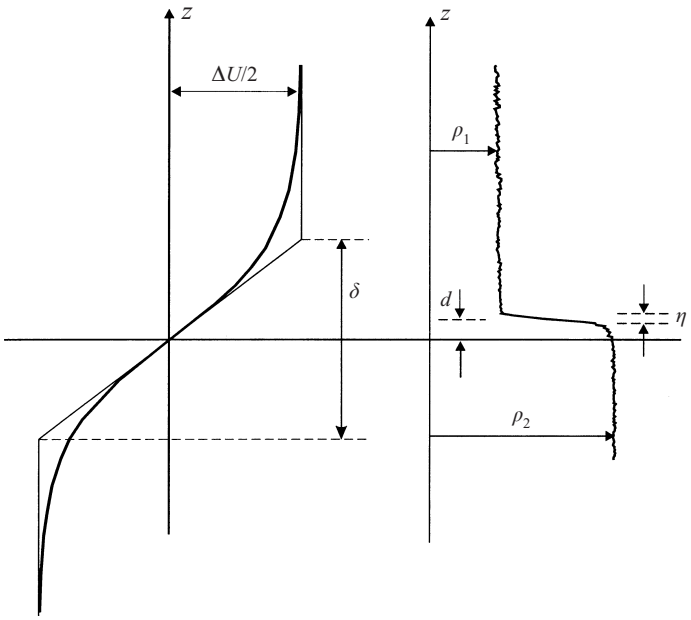


FIGURE 1. Definition diagram making use of laboratory measurements of velocity and density profiles in an exchange flow. δ and η are the thickness of the shear layer and the density layer, respectively.

The present paper examines Holmboe instabilities observed in a laboratory model of exchange flow over an obstacle. Measurements are compared with recent theoretical and numerical studies. A review of the literature is presented in § 2. The details of the experiments are discussed in § 3. Section 4 presents an account of the evolution of the mean flow and of the interfacial instabilities. Section 5 compares the experimental results with numerical studies. Concluding remarks are presented in § 6.

2. Literature review

In this section we review studies of hydrodynamic instabilities, particularly Holmboe's instability, in sheared two-layer flows. The variation of velocity and density in a typical two-layer flow is presented in figure 1. The interfacial region between the two layers is characterized by the shear layer thickness (sometimes known as the 'vorticity thickness'), $\delta = \Delta U/(\partial U/\partial z)_{\max}$, and the density layer thickness, $\eta = \Delta\rho/(\partial\rho/\partial z)_{\max}$, where U and ρ are the velocity and density respectively, and ΔU and $\Delta\rho$ are the velocity and density differences between the two layers. Many studies of stably stratified shear flows have assumed that $\eta \approx \rho$, in which case the primary mode of instability is the Kelvin–Helmholtz (K–H) instability, consisting of a series of billows travelling with a phase speed equal to the mean velocity, see Turner (1973). However, applying linear stability analysis to piecewise linear profiles, Holmboe (1962) predicted that for inviscid flows with $R \equiv \delta/\eta \gg 1$, another type of instability, which now bears his name, is generated. Holmboe's instability is characterized by two sets of waves, one set cusping into the upper layer and the other into the lower layer. These waves have the same growth rate and wave speed, but propagate in opposite directions with respect to the mean flow velocity.

https://doi.org/10.1017/S002211200000286X Published online by Cambridge University Press

Holmboe (1962) found that for inviscid flows Holmboe instabilities could occur for any positive bulk Richardson number, $J = g'\delta/(\Delta U)^2$, while Kelvin–Helmholtz instabilities can only occur when $J < 0.07$, where $g' = g(\rho_2 - \rho_1)/\rho_2$ is the reduced gravity, with ρ_1 and ρ_2 being the densities of the upper and lower layers respectively. Haigh & Lawrence (1999) further showed that while Kelvin–Helmholtz instabilities are possible in the range $0.046 < J < 0.071$, Holmboe instabilities have a larger growth rate in that range. Hazel (1972) extended Holmboe's analysis by allowing a finite density layer thickness. He found that Holmboe instabilities appear when $R > 2$. Assuming hyperbolic tangent profiles for both the shear and density layers Smyth & Peltier (1989) showed that R must be larger than 2.4 for Holmboe instabilities to be generated.

Browand & Winant (1973), Koop (1976), and Lawrence, Browand & Redekopp (1991) performed mixing-layer experiments under conditions that might have been expected to yield Holmboe's instability, but their flows were 'one-sided' in that only one train of waves was evident. Lawrence *et al.* (1991) concluded that this one-sidedness was a result of the boundary layers that formed on either side of the splitter plate causing a vertical shift between the centres of the velocity and density interfaces. They incorporated a shift parameter, $\varepsilon = 2d/\delta$, where d is the vertical shift, see figure 1. When the shift ε increases, the stability boundaries for the two sets of waves bifurcate, with the growth rate of one set increasing, and that of the other decreasing. Pouliquen, Chomaz & Huerre (1994) found that the shift could also be caused by the surface tension between two immiscible fluids. Yonemitsu *et al.* (1996) also pointed out that non-symmetric Holmboe instabilities can be caused by the proximity of a boundary.

While inviscid theories predict that the flow is unstable to Holmboe instabilities for any positive J, viscosity stabilizes the instabilities when the shear Reynolds number, $Re = \Delta U\delta/\nu$, is sufficiently small. Browand & Wang (1972) and Browand & Winant (1973) found that in their laboratory experiments, where $Re < 100$, the growth rates of the Holmboe instabilities were an order of magnitude smaller than inviscid predictions. Nishida & Yoshida (1987) incorporated the effect of viscosity in their numerical studies using a hyperbolic-tangent velocity profile and a two-layer step density profile with $\varepsilon = 0$. They found that a critical Richardson number existed for Holmboe instabilities, above which the flow is stable. This critical Richardson number increases from 0.66 to 0.77 when the Reynolds number is increased from 800 to 4000. Yonemitsu *et al.* (1996) considered flows with a shift and found that the critical Richardson number is increased due to the increase of the growth rate of one set of Holmboe waves. Koop & Browand (1979) and Yonemitsu (1991) also noticed the existence of a critical Richardson number in their laboratory experiments.

Including both viscosity and diffusivity and using hyperbolic-tangent velocity and density profiles, Smyth, Klaassen & Peltier (l988) found that the diffusivity does not qualitatively change the stability boundaries, but diffusion alters the magnitude of the growth rate to a substantial degree. Haigh (1995) furthered this study by allowing a shift, and showed that compared to the piecewise-linear profiles of Lawrence *et al.* (1991), the stability boundaries for the smooth profiles open up, also the difference between the growth rates of the two sets of waves increases.

The nonlinear evolution of Holmboe's instability was studied numerically by Smyth *et al.* (1988) and Smyth & Peltier (1989) for viscous and diffusive flows using unshifted hyperbolic-tangent profiles for both density and velocity. Smyth *et al.* (1988) also confirmed the prediction of Holmboe (1962) that wave speeds vary when positive and negative waves pass through each other. Haigh (1995) furthered this study for

https://doi.org/10.1017/S002211200000286X Published online by Cambridge University Press

shifted flows and found that wave speeds increase slightly as nonlinear effects become important.

In the above studies, the instabilities were typically assumed to be two-dimensional. This is generally justified since they will normally pass through a distinct two-dimensional state before becoming dependent on the third spatial coordinate. However, Smyth & Peltier (1990, 1991) found that the fastest-growing Holmboe instability can be three-dimensional for a limited range of shear Reynolds numbers and Richardson numbers. Observations of three-dimensional Holmboe waves have been reported by Moore & Long (1971), Koop & Browand (1979) and Sargent & Jirka (1987), but these flows may have initially been two-dimensional with the three-dimensional disturbances developing later.

Despite recent advances in theoretical and numerical studies, good experimental realizations of Holmboe instabilities have been limited. Lawrence *et al.* (1991) explained the difficulty in obtaining symmetric Holmboe waves in mixing-layer experiments as a result of the shift of the density and velocity interfaces caused by the splitter plate. The tilting tube experiments of Pouliquen *et al.* (1994) generated symmetric Holmboe instabilities, but did not last long enough for a detailed study of wave development. Nor did the arrested saline-wedge experiments of Yonemitsu *et al.* (1996) allow a detailed study of Holmboe instabilities. In the present paper we present the results of laboratory experiments which, although not initially designed to do so, have provided an excellent opportunity to study Holmboe's instability.

3. Experiments

3.1. *Experimental design*

Exchange flow experiments were conducted in a 370 cm long, 106 cm wide and 30 cm deep tank. The tank was divided into two reservoirs which were connected by a narrow channel of constant width, $b = 10$ cm. A plan view of the tank is given in figure 2(*a*), and figures 2(*b*) and 2(*c*) are side views of an actual experiment. An underwater sill was placed in the left-hand portion of the channel. The sill height is given by

$$h(x) = h_s \cos^2\left(\frac{\pi x}{2L_s}\right) \quad \text{for} \quad \left|\frac{x}{L_s}\right| \leqslant 1, \tag{1}$$

where $h_s = 8$ cm is the sill height at its crest, and $L_s = \pi h_s = 25$ cm is the sill half-length.

Experiments were initiated by removing a thin plate that was inserted in the connecting channel to separate the fluids of different density in the reservoirs. The parameters for each of the experiments are given in table 1. Experiments 2–7 were performed with salt as the stratifying agent, a total water depth $H = 28.0$ cm, and $L = 103$ cm, where L is the distance from the crest of the sill to the right-hand end of the channel. The only variable that was changed between these experiments was the reduced gravity g'. Varying the reduced gravity permitted an examination of Reynolds number effects, since the flow velocities scale with the square root of g'. Two additional experiments were performed, one (experiment 1) with a longer channel ($L = 175$ cm), and one (experiment 8) with temperature as the stratifying agent. Although the longer channel provided more opportunity for Holmboe instabilities to develop, it was not used extensively due to the difficulty in obtaining simultaneous measurements of velocity and density fields over a significant portion of its length. The temperature-

https://doi.org/10.1017/S002211200000286X Published online by Cambridge University Press

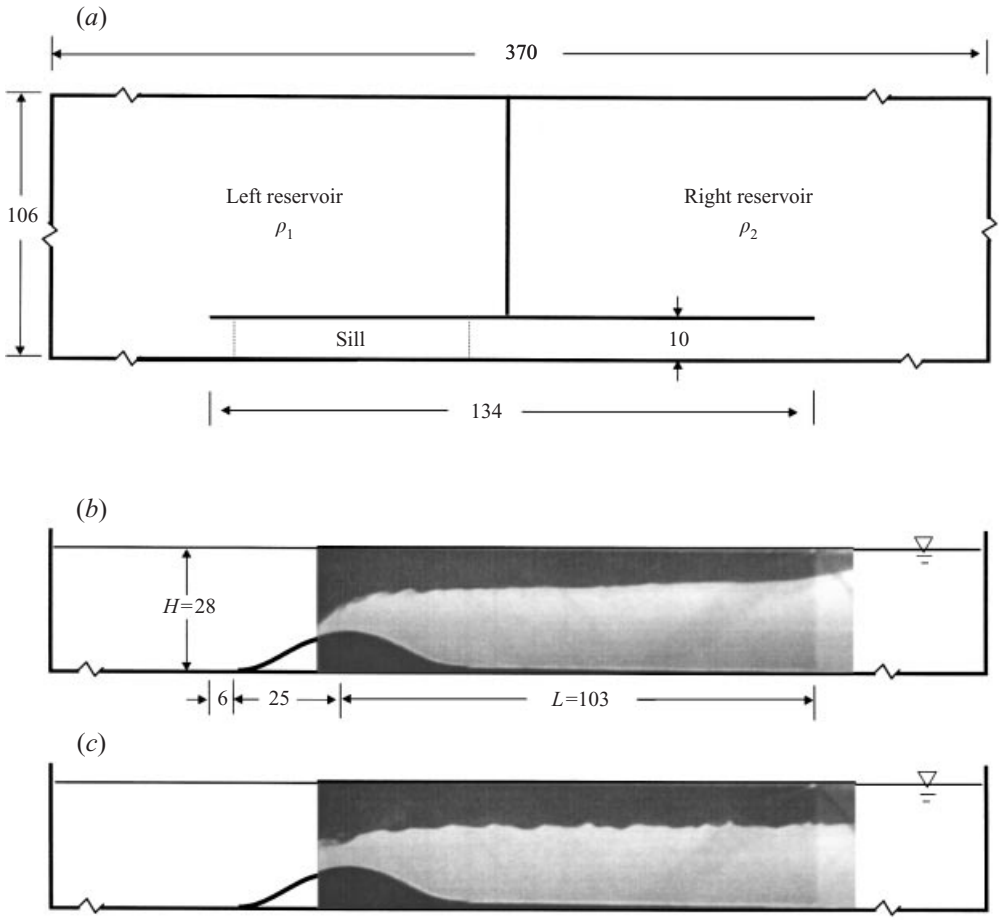


FIGURE 2. (*a*) Plan view of the experimental setup. (*b*, *c*) Side views of experimental setup including photographs of experiment 3 taken during (*b*) steady maximal exchange at $t = 0.5$, and (*c*) sub-maximal exchange at $t = 1.0$. All dimensions are in centimetres.

stratified flow provided an opportunity to examine the effects of changing R, the ratio of the vorticity thickness to the thickness of the density interface.

The characteristic time scale, T, for the experiments is equal to the total volume of water in the tank, $V = AH$, where A is the surface area of the tank, divided by the characteristic flow rate, $Q = (g'H)^{1/2}Hb$, i.e. $T = (A/b)/(g'H)^{1/2}$. This time scale varies between 210 s (experiment 7) and 710 s (experiment 2), see table 1. For the remainder of this paper time will be non-dimensionalized with respect to T. Horizontal distance will be non-dimensionalized with respect to L, so that $x = 0$ at the crest of the sill and $x = 1$ at the right-hand end of the connecting channel.

3.2. *Measurement techniques*

The measurement techniques used in this study are outlined below; additional details are given in Zhu (1996). A laser sheet, obtained by splitting the laser beam from a 5 W argon-ion laser using a scanning mirror, was used to illuminate the flow from above. The velocity field of the flow was obtained by tracking the movements of neutrally buoyant Pliolite particles in the light sheet. The movements of the particles were recorded using a low-noise CCD camera and the images were stored on an Hi

https://doi.org/10.1017/S002211200000286X Published online by Cambridge University Press

Experiment	g' cm s^{-2}	Pr	L (cm)	H (cm)	T (s)
1	1.60	700	175	28.5	581
2	1.09	700	103	28.0	710
3	1.56	700	103	28.0	593
4	2.34	700	103	28.0	485
5	3.12	700	103	28.0	420
6	6.24	700	103	28.0	297
7	12.5	700	103	28.0	210
8	2.50	8	103	28.0	469

TABLE 1. List of experiments. T is the characteristic time scale, $T = (A/b)/(g'H)^{1/2}$, where $A(= 3.92\,\mathrm{m}^2)$ is the surface area of the tank, and $b = 10\,\mathrm{cm}$ is the width of the channel. The density difference in experiment 8 was obtained using cool (16 °C) and warm (27 °C) water.

8 mm video camera. The density interface between the two layers was visualized by dissolving Rhodamine WT dye into the lower layer, and recorded using a Super-VHS camera. The images were captured by a personal computer using a frame grabber board for subsequent image processing.

In all experiments simultaneous velocity and interface information was obtained by adding Rhodamine WT dye and Pliolite particles to the flow. A green filter was used to highlight the particles, and an orange filter was used to highlight the dyed lower layer. Using filters, high-quality images of particles and dye were recorded onto separate videotapes. The velocity fields were obtained by following particle 'patterns' between successive images using the maximal cross-correlation technique (Stevens & Coates 1994). The location of the density interface was obtained by determining the maximum gradient of light intensity between the transparent upper layer and the dyed lower layer. In determining the shift of the density interface from the shear centre, images of particles and dye were recorded onto the same video image to avoid possible errors resulting from dealing with two video images. In this case, the dye concentration was reduced to avoid obscuring the particles.

Density profiles were taken using a conductivity probe. The probe, driven by a computer-controlled stepper motor, sampled only on downward traverses, as it entrained a small amount of denser fluid during upward traverses. The probe was traversed slowly ($0.5\,\mathrm{cm\,s}^{-1}$) to minimize disturbances and to increase the spatial resolution. Output of the conductivity probe was digitized using a l2-bit A/D board. The measured voltage data were converted first to conductivity, then to salinity, and finally to density. A typical density profile is given in figure 1.

In addition to the measurements obtained using a conductivity probe, the thickness of the interfacial mixing layer was also visualized by using the chemical reaction technique of Breidenthal (1981). Phenolphthalein, a common pH indicator, reacts with a base and generates a red product. The transition interval of phenolphthalein is from pH = 8 (clear) to pH = 10.5 (red). Phenolphthalein was added into the fresh water reservoir together with a small amount of HCl to make the water slightly acid (pH $\approx$ 6). Sodium hydroxide was added into the salt-water reservoir to give a pH of 11.7. Therefore, across the interfacial mixing layer, the pH changed from 6 to 11.7, with a red layer indicating fluid with $8 < \mathrm{pH} < 11.7$. The thickness of this red layer correlated well with the thickness of the interfacial mixing layer, η, as measured using the conductivity probe. This chemical reaction technique had the advantage of

https://doi.org/10.1017/S002211200000286X Published online by Cambridge University Press

allowing us to estimate the thickness of the interfacial mixing layer non-intrusively and continuously during the experiment.

3.3. *Experimental errors*

In the following sections we will be concerned with the errors in J, Re, ε, the non-dimensional wavenumber $\alpha = 2\pi\delta/\lambda$ where λ is the wavelength, and the non-dimensional wave speed $c_r^{\pm} = (c_r^{\pm^*} - \bar{U})/(\frac{1}{2}\Delta U)$ where $c_r^{\pm^*}$ is the dimensional wave speed of either the positive or negative waves, and the mean velocity $\bar{U} = \frac{1}{2}(U_1 + U_2)$. The most important sources of error in determining these parameters were those involved in measuring the shift between the centres of the density and velocity interfaces d, the vorticity thickness δ, the velocity shear ΔU, and the mean velocity $\bar{U}$. Each of these measurements is dependent to some degree on the resolution of the video images. Each 40 cm (horizontal) by 30 mm (vertical) image contains 640×480 pixels, giving a pixel resolution of 0.06 cm.

In determining the velocity profile the time interval between two images was chosen to ensure that particles had an average travel distance of approximately 20 pixels (1.2 cm), resulting in an error in ΔU of approximately 5% due to pixel resolution. This error was reduced to approximately 3% by averaging 3 or 4 neighbouring velocity profiles. Similarly the error in determining the mean velocity $\bar{U}$ was approximately 3% of ΔU

The thickness of the shear layer δ, and the position of its centre were determined from velocity profiles. Errors in the estimates of both ΔU and the maximum velocity gradient contribute to the error in estimating δ. Analysis of the combined error is difficult and likely to be imprecise. However, we noted that throughout the duration of each experiment measurements of δ were subject to random fluctuations of up to 10% about a constant mean value. For the remainder of this study we will assume a constant value of δ, subject to a 10% error. The shift between the centres of the density and velocity interfaces, d, is subject to an error of approximately 2 pixels (0.12 cm). The thickness of the density interface η, as determined from the chemical reaction described above, is subject to an error of approximately 1 pixel.

Given the above analysis our estimates of $J, Re, c_r^{\pm}$ and α are typically subject to 10–15% errors. For a typical value of δ of 4.5 cm we are able to estimate ε to within ± 0.06. Our measurements of η are subject to an error of up to 33% since the density interface is as thin as 3 pixels. However, this is of no concern since we shall see that when η is small the interfacial thickness ratio, R, is much larger than the critical value for the growth of Holmboe's instability.

4. Flow evolution

Experiments were initiated by removing a thin plate, which separated lighter fluid in the left reservoir from denser fluid in the right reservoir. Upon removal of the plate, two gravity currents form. The flow is unsteady until the transients associated with these gravity currents dissipate. A brief summary of the subsequent evolution of the mean flow is given here; for a detailed account of the hydraulics of the mean flow see Zhu & Lawrence (2000).

4.1. *Evolution of the mean flow*

Once the initial transients have died down a steady flow is established (figure 2*b*) with two internal hydraulic controls, one at the sill crest (crest control) and one at the right-hand end of the channel (exit control). The crest control acts in a similar manner as

https://doi.org/10.1017/S002211200000286X Published online by Cambridge University Press

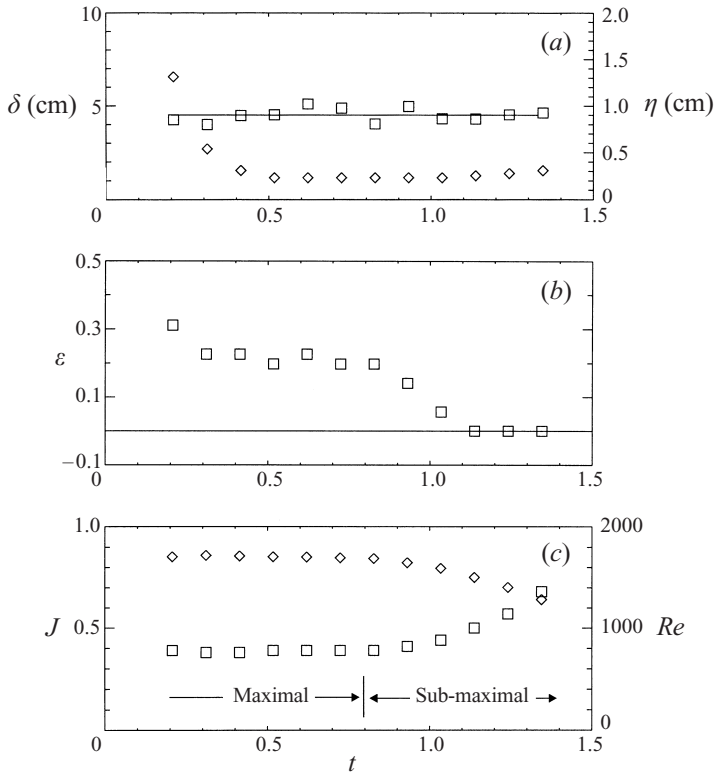


FIGURE 3. Evolution of the mean flow with time in experiment 1 measured at $x = 0.6$. (*a*) $\delta(\square)$ and η ($\diamond$); ———, average shear layer thickness, $\delta = 4.5\,\text{cm}$. (*b*) The non-dimensional shift ε. (*c*) $J(\square)$ and Re ($\diamond$).

that in crest-controlled single-layer flows. The sill crest separates internally subcritical flow on its right from internally supercritical flow on its left, and the lower layer thins as it passes over the sill crest. The presence of an exit control is characterized by a thinning of the upper layer at the right-hand end of the channel (figure 2*b*), and results in a 'maximal' exchange flow. Eventually, the exit control is submerged as the interface level in the right-hand reservoir drops due to the accumulation of less-dense water (figure 2*c*). This results in a reduced 'sub-maximal' exchange flow, which gradually weakens throughout the remainder of the experiment.

During sub-maximal exchange flow a region of almost parallel flow is established in the right-hand portion of the channel, extending from the right-hand end of the sill to the right-hand end of the channel (figure 2*c*). In this region there is a gradual rise in interface level due to frictional effects. We will focus on this region, because the results of previous theoretical studies of hydrodynamic instability are most likely to apply within it. The flow is also almost parallel in the right-hand portion of the channel during maximal exchange flows, except at the extreme right-hand end where the interface curves upwards (figure 2*b*) and non-hydrostatic effects become important, as discussed in Zhu & Lawrence (2000).

A number of mean flow parameters affect the stability of the interface, including $\eta, \delta, \varepsilon, J$, and Re. The variation of each of these parameters, measured at $x \approx 0.6$ during experiment 1, is presented in figure 3. The same qualitative behaviour was

https://doi.org/10.1017/S002211200000286X Published online by Cambridge University Press

observed in all of the experiments. The density thickness, η, decreases rapidly at the start of the experiment, presumably as mixed fluid generated during the start-up of the exchange is advected out of the channel. Once this fluid has been removed η remains relatively constant. Within the bounds of experimental error the vorticity thickness δ is 4.5 cm, for the duration of the experiment. In subsequent calculations we will use this value. The vertical shift between the density and velocity interfaces, ε, decreases from about 0.3 to 0 during the experiment. The Richardson number, J, is constant during the period of maximal exchange ($T \approx 0.2$–0.8), but then increases as the velocity difference decreases during the period of sub-maximal exchange. Similarly, the shear Reynolds number is initially constant, but then decreases once the velocity difference starts to decrease. The variation in each of the above parameters provides us with an excellent opportunity to test theoretical and numerical predictions of interface behaviour against our observations.

4.2. *Evolution of interfacial instability*

The time evolution of interfacial instability is illustrated graphically using a wave characteristics plot. A time sequence of the interface height for $0.5 < x < 1.0$, and $0.21 < t < 1.45$ is displayed in an x, t plot (figure 4), similar to that used in open channel flows (Henderson 1966). The interface elevation at each point in the (x, t)-plane is represented as a grey scale, with the bright and dark points representing high and low interface elevations respectively. Thus, the characteristics of the positive waves (upward cusps) and the negative waves (downward cusps) appear as oblique bands of light and dark. Note, these waves are fluctuations about a 'mean' interface level that rises gradually in the x-direction, and falls slowly during the period of sub-maximal flow. Changes in the 'mean' interface elevation were obtained by dividing the data into one-minute segments. Within each segment a best fit to the data was obtained while assuming that the interface level changed linearly with time, and that the variation with position was independent of time. Although this procedure was very effective, small imperfections are evident from the changes in shading between the one-minute segments in figure 4.

A measure of the level of wave activity is the variance of the interfacial elevation from its mean value, i.e.

$$\sigma_y^2 = \frac{1}{x_2 - x_1} \int_{x_1}^{x_2} (y - \bar{y})^2 \, \mathrm{d}x, \tag{2}$$

where y and $\bar{y}$ are the instantaneous and mean interface position respectively, and x_1 and x_2 are the boundaries of the region of interest. The change of σ_y^2 against time where $x_1 = 0.5$ and $x_2 = 0.8$ is plotted in figure 5 for experiment 1. Upon the establishment of maximal exchange ($t \approx 0.2$) the variance was very low, it increased to a peak at $t \approx 1.0$, and then decreased to almost zero by $t \approx 1.4$, which is consistent with the wave characteristics plot (figure 4).

The ratio of the interfacial thicknesses, R, is too low for instabilities to form in the right-hand portion of the channel prior to $t \approx 0.3$. Weak positive waves are observed, but these were generated in the vicinity of the sill where R was presumably higher. At about $t \approx 0.3$, R increases to the point where negative instabilities form. Positive waves do not form, or grow, in the right-hand portion of the channel at this time, because $\varepsilon \approx 0.2$ (figure 3*b*) strongly favouring the growth of negative instabilities (Lawrence *et al.* 1991). Note that, even though these negative waves travel to the right during the period of maximal exchange ($0.2 < t < 0.8$), they have a negative celerity with respect to the mean flow velocity.

https://doi.org/10.1017/S002211200000286X Published online by Cambridge University Press

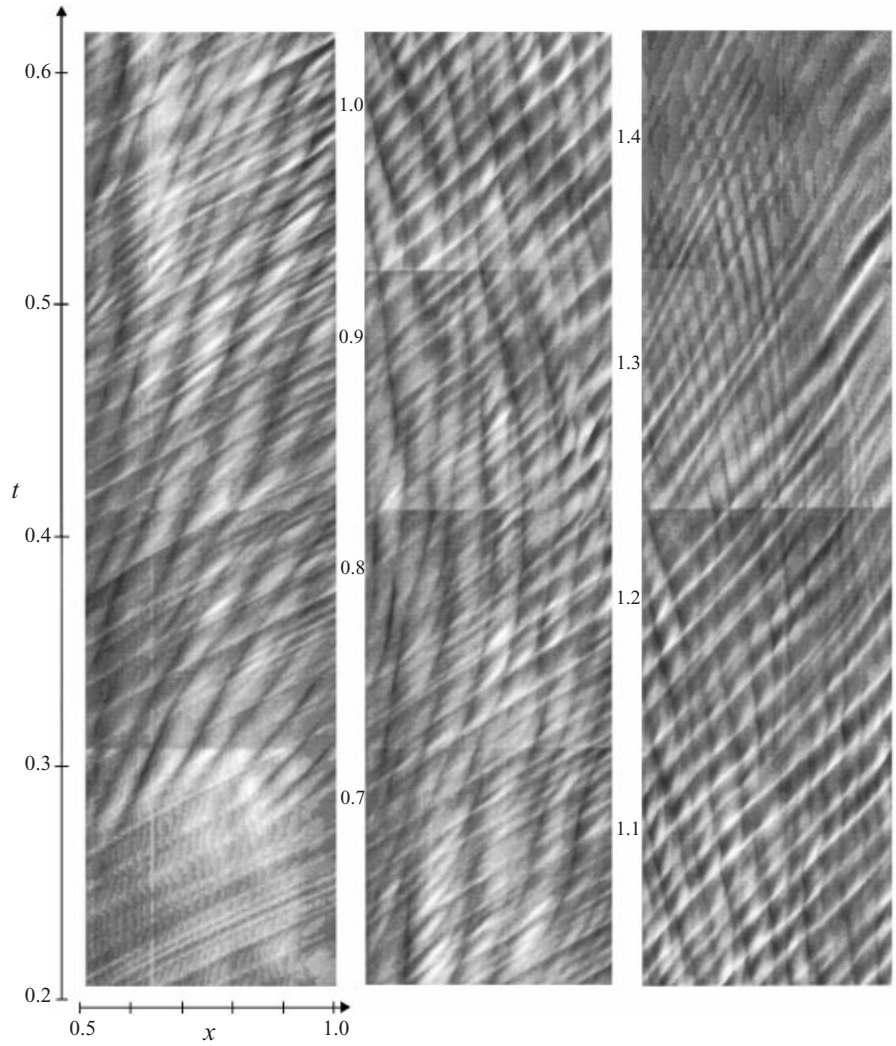


FIGURE 4. Characteristics of Holmboe waves for experiment 1 in the region $x = 0.5$–1.0 during the period $t = 0.21$–1.45. The left, middle and right-hand strips represent $t = 0.21$–0.62, 0.62–1.03, 1.03–1.45, respectively. Each strip contains 240 rows, with each row representing the interface position along the channel. The intensity is a measure of the height of the interface: brighter shading for a higher interface. Oblique bands of dark and light show the propagation of positive and negative waves respectively.

Once the flow becomes sub-maximal ($t \approx 0.8$) the lowering of the interface level results in a reduction in the upper-layer flow speed and an increase in the lower-layer speed, so that even though the mean velocity is always to the right, its magnitude decreases with time. This results in a steepening of the positive wave characteristics. The negative wave characteristics steepen until the point where they change direction. So the negative waves start to flow to the left. Between $t \approx 0.8$ and $t \approx 1.1$, the interfacial shift ε drops from 0.2 to 0, with the result that negative waves are no longer favoured. Figure 4 shows a corresponding increase in the relative strength of the positive waves, until it matches that of the negative waves. It is at this time that symmetric Holmboe instabilities are clearly observed.

https://doi.org/10.1017/S002211200000286X Published online by Cambridge University Press

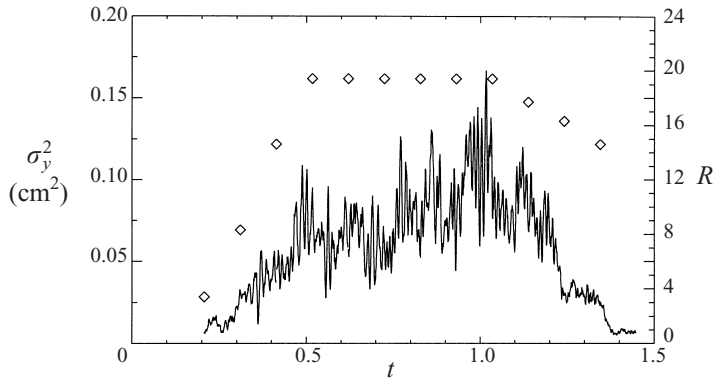


FIGURE 5. Evolution of interfacial wave activity in experiment 1: ——, variance (σ_y^2) of the short-term interfacial fluctuations measured between $x = 0.5$ and 0.8; ◇, thickness ratio $R = \delta/\eta$.

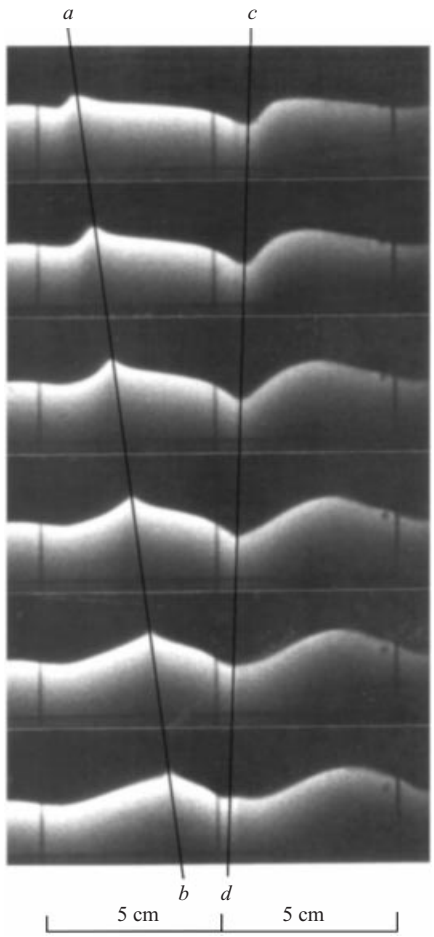


FIGURE 6. Series of photos showing Holmboe instabilities observed in experiment 1, taken at $x \approx 0.6$ and starting at $t \approx 1.1$ with $J \approx 0.5$, $Re \approx 1600$ and $\bar{U} \approx 0.4\,\mathrm{cm\,s^{-1}}$. The photographs were taken at 0.42 s intervals starting from the top.

https://doi.org/10.1017/S002211200000286X Published online by Cambridge University Press

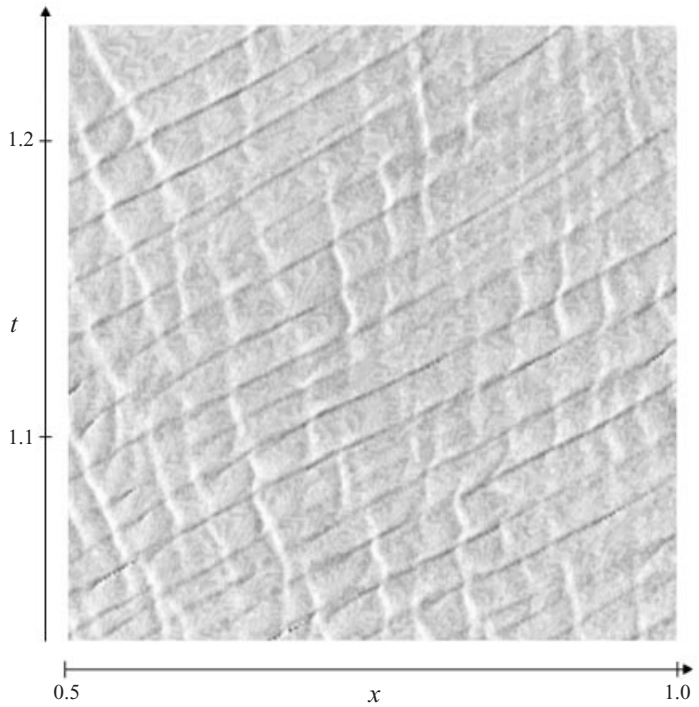


FIGURE 7. Characteristics diagram showing changes in the speed of the negative waves as they pass through positive waves in experiment 1 in the region $x = 0.5$–1.0 at $t = 1.03$–1.24. The positive and negative waves are seen as the dark and bright bands respectively.

A series of six photographs of the symmetric Holmboe instabilities observed in experiment 1 is presented in figure 6. These photographs are taken at 0.42 s intervals at $x \approx 0.6$ and $t \approx 1.1$. The propagation of a positive (upward cusping) wave crest at approximately $1.2\,\mathrm{cm\,s^{-1}}$ to the right is traced by the line *a*–*b*, and the propagation of a negative (downward cusping) wave crest at approximately $0.3\,\mathrm{cm\,s^{-1}}$ to the left is traced by the line *c*–*d*. Given that the mean velocity of the flow is approximately $0.4\,\mathrm{cm\,s^{-1}}$ to the right, the waves are propagating at about the same speed, but in opposite directions, with respect to the mean flow. The positive and negative waves also have approximately equal amplitude. This symmetric behaviour is notable since it was not realizable in mixing-layer experiments (Lawrence *et al.* 1991). The occurrence of symmetric behaviour is due to the shift between the velocity and density interfaces, ε, vanishing towards the end of the experiment, as illustrated in figure 3.

It is of interest to examine variations in wave speed as they pass through each other. Holmboe (1962) predicted that the waves speed up when they approach each other and slow down when they are far apart. This result was confirmed in the linear numerical simulations of Smyth *et al.* (1988) and Haigh (1995). In our experiments variations in the speed of negative waves are evident if we focus on the characteristics plot for $x = 0.5$–1.0 and $t = 1.03$–1.24 (figure 7). However, our observations do differ from earlier predictions. The observed speed of the positive waves does not vary. The negative waves appear to slow down as they pass through the positive waves, and to speed up when they are furthest from the positive waves. Haigh's (1995) nonlinear predictions more closely match our observations of the negative waves. However, further investigation is required.

https://doi.org/10.1017/S002211200000286X Published online by Cambridge University Press

Towards the end of the experiment the lowering of the interface in the right-hand reservoir resulted in a diminishing flow rate, resulting in a decrease in Re, an increase in J (figure 3*c*), and a stabilization of the interface. From figure 4 we also see that the wavelength of the instability decreases, as predicted, with increasing J (Lawrence *et al.* 1991). By $t \approx 1.4$ when $J \approx 0.7$ and $Re \approx 1200$, the instabilities had almost vanished, as evidenced by the reduction in grey-scale variations in figure 4, and in the negligible variance of the interfacial elevation plotted in figure 5.

The above results show how the evolution of the interfacial instabilities is consistent with the time variation of the mean flow parameters. We will now examine some of the properties of the instabilities more closely, making comparisons with numerical and theoretical predictions.

5. Comparison of laboratory measurements with numerical predictions

In the previous section we discussed the flow evolution and the development of interfacial instabilities in experiment 1, which was performed in the long flume ($L = 175$ cm). Subsequent experiments were performed in a short flume to facilitate a better resolution of the flow field. Six additional experiments (experiments 2–7) investigated the effects of increasing Re, and a final experiment (experiment 8) examined the effect of using heat rather than salt as the stratifying agent.

5.1. *Effects of heat rather than salt as the stratifying agent*

Experiment 8 was performed using warm and cold water to obtain approximately the same density difference as in experiment 4 (table 1). In all other respects the setup of the two experiments was the same. The impact of the change in stratifying agent is dramatically illustrated in figure 8. The interfacial instabilities observed in the salt-stratified flow (experiment 4) never develop in the thermally stratified flow (experiment 8). In each of the experiments the interface thickness ratio R was low initially, as in experiment 1 (figure 5). In experiment 4 the interface thickness ratio rose to about 20 after the initial start-up, whereas R remained low throughout experiment 8. This is because the Prandtl number (Pr) for the salinity-stratified flow was about 700, whereas for the temperature-stratified flow $Pr \approx 7$ ($Pr = 6$ for the upper layer, and $Pr = 8$ for the lower layer). Smyth *et al.* (1988) showed that the thickness ratio R approaches $\sqrt{Pr}$ given sufficient time. Given that numerical studies by Smyth *et al.* (1988) and Haigh (1995) show that R must be greater than about 2.4 for Holmboe's instability to form, it is not surprising that the thermally stratified interface remained stable. Similarly, Holmboe instabilities are not observed in stratified air flows since $Pr \approx 1$. This is confirmed by the air flow experiments of Scotti & Corcos (1972) where Kelvin–Helmholtz instabilities were observed when J was small, and the flow was stable when J was large.

5.2. *Effects of J and Re on Holmboe's instability*

To test effects of J and Re on Holmboe's instability we recorded whether or not the interface was stable at regular time intervals throughout each of the eight experiments at $x = 0.6$. The hydraulics of the flow are such that at $x = 0.6$, $J \gg 0.07$, and Kelvin–Helmholtz instabilities cannot form. The presence, or otherwise, of Holmboe instabilities is indicated in figure 9 for experiments 1–7. The results for experiment 8 are omitted, as are those during the start-up phase of each of the other experiments, since low values of R ensure stability.

We can relate the results for experiment 1 to the data given in figures 3–5. The

https://doi.org/10.1017/S002211200000286X Published online by Cambridge University Press

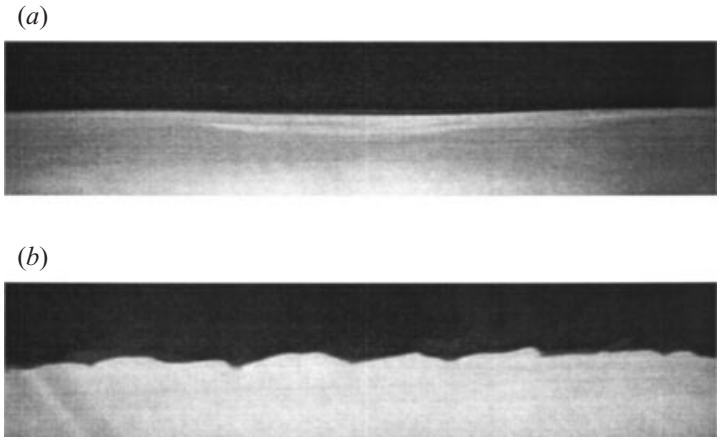


FIGURE 8. Observations of the interface in thermally and salinity-stratified flow experiments. (*a*) Thermally stratified flow (experiment 8) with $T_1 = 27\,^{\circ}\mathrm{C}$, $T_2 = 16\,^{\circ}\mathrm{C}$, $J \approx 0.35$ and $Re \approx 1800$. (*b*) Salinity-stratified flow (experiment 4), with $J \approx 0.35$ and $Re \approx 2200$.

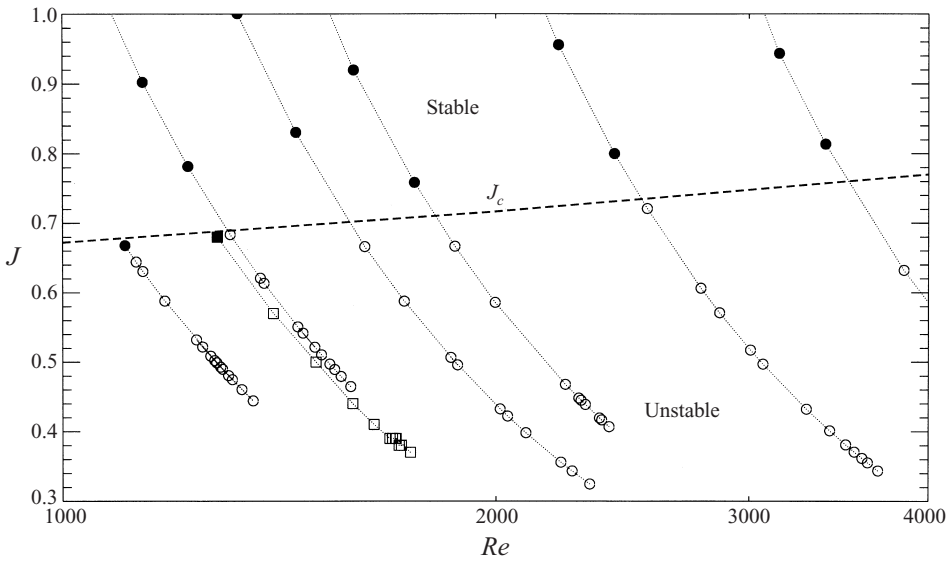


FIGURE 9. Stability criteria for Holmboe's instability. Open symbols: Holmboe's instability observed; solid symbols: Holmboe's instability not observed; ——, stability boundary from Nishida & Yoshida (1987). The data for experiments 2 to 7 appear on curves reflecting the increase in J and decrease in Re with time. The curve for experiment 2 is to the left, and experiments 3 to 7 have increasingly higher Re. Data from experiment 1 are also plotted as squares.

data were obtained at 1 minute intervals ($\Delta t = 0.103$) from 2 minutes ($t = 0.21$) until 13 minutes ($t = 1.34$) after the start of the experiment. The first point ($t = 0.21$) is not plotted on figure 9, because at this time R is too low for Holmboe's instability to form. From this point until $t = 1.14$, both figures 4 and 5 show that the interface is unstable. By $t = 1.24$ the level of interfacial variance has dropped, but we still classify the flow as unstable because figure 4 indicates that there still is some wave growth at $x \approx 0.6$. However, by $t = 1.34$ the flow instabilities are decaying at $x = 0.6$, and we have classified the flow as stable at this point and time. It is worth noting that

https://doi.org/10.1017/S002211200000286X Published online by Cambridge University Press

there is some wave growth at about $x = 0.9$ at this time, which can be attributed to changes in the flow near the end of the channel. At $t = 1.34$, $J \approx 0.67$ and $Re = 1300$, the flow stabilizes, which is consistent with the results of Nishida & Yoshida (1987) that the critical value of the Richardson number is $J_c = 0.68$ when $Re = 1300$.

The results for experiments 2–7 are also consistent with the predictions of Nishida & Yoshida (1987). This is not surprising since their analysis assumed $\varepsilon = 0$, which is in fact the case towards the end of the experiments when the stability transition occurs (figure 3*b*). However, we were not able to provide conclusive confirmation of the result that J_c increases with increasing Re, because of the difficulties involved in providing a precise estimate of J_c in our experiments.

Some previous studies (Keulegan 1949; Grubert 1989) found the stability of density interfaces to be determined by the Keulegan number, $K = (\Delta U)^3/g'\nu$. The onset of instabilities for a laminar flow, as judged by the appearance of waves at the interface, occurred when K exceeded a critical value of about 500 (Keulegan 1949). We can apply the Keulegan number to the present study by noting that $K = Re/J$. According to Nishida & Yoshida's (1987) numerical studies, and our experimental observations, J_c changes only slightly from about 0.66 to 0.77 when Re increases from about 800 to 4000, implying that the critical value for K increases from about 1200 to 5200. Thus K is not a good indicator of Holmboe's instability. The Keulegan number is only appropriate when there are no imposed length scales (see Turner 1973, p. 112), whereas the vorticity thickness is important in the study of Holmboe's instability.

5.3. *Measurements and predictions of wavenumber and wave speed*

Holmboe (1962) analysed the linear stability of the two-dimensional flow of two unbounded, inviscid layers subject to a piecewise-linear velocity distribution centred about a sharp density interface. Strictly speaking, none of these conditions apply in our experiments. The layers are bounded, with one layer being thinner than the other, the velocity and density distributions are continuous, the fluids are viscous, and the density interfaces are displaced. Furthermore, the flow becomes nonlinear and is unsteady. Extensions to Holmboe's analysis accounting for a number of these effects have been made, as discussed in § 2. Despite the fact that short of a direct numerical simulation we cannot hope to model our experiments exactly, it is instructive to make some comparisons between theory and laboratory measurements.

If we use Holmboe's analysis without any of the extensions discussed above, the comparison with the wavenumbers, α, of the instabilities is surprisingly good. The wavenumbers of the negative and positive waves measured during experiments 3 and 4 are plotted against J in figure 10, together with the stability boundaries and the maximum growth rate curve from Holmboe's analysis. The wavenumbers are all within the range predicted for instabi1ity. Figure 11 shows that Holmboe's analysis also predicts the wave speeds of the positive waves well, but not the negative wave speeds.

The parameters for experiments 3 and 4 fall within ranges where we might expect extensions to Holmboe' s analysis to be needed. At the start of each experiment $\varepsilon \approx 0.25$ (figure 12), a value at which the stability diagram is substantially affected (Lawrence *et al.* 1991). Similarly, the thickness of the upper layer is less than twice the vorticity thickness (δ) and the thickness of the lower layer is approximately 4δ. Haigh & Lawrence (1999) have shown that the stability diagram changes when the thickness of each layer is less than 2.5δ in a flow with layers of equal thickness. Yonemitsu *et al.* (1996) predict changes in a flow with one bounded and one unbounded layer when the thickness of the bounded layer is less than 3δ. Finally, Haigh (1995) and

https://doi.org/10.1017/S002211200000286X Published online by Cambridge University Press

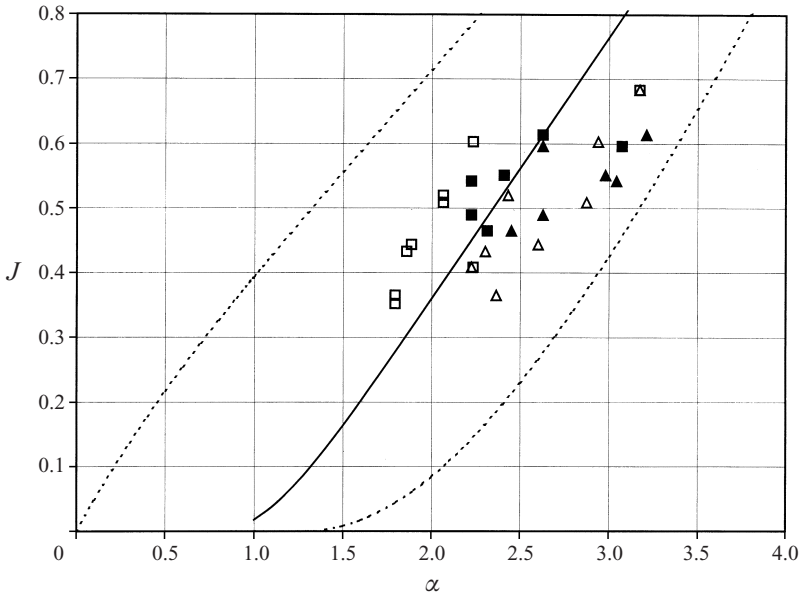


FIGURE 10. Comparison of measured wavenumbers in experiments 3 and 4 with Holmboe's (1962) predictions. The solid line gives the curve of maximum growth rate, and the dashed lines give the stability boundaries. Squares and triangles indicate measurements of positive and negative waves, respectively. Data from experiments 3 and 4 are indicated by solid and open symbols, respectively.

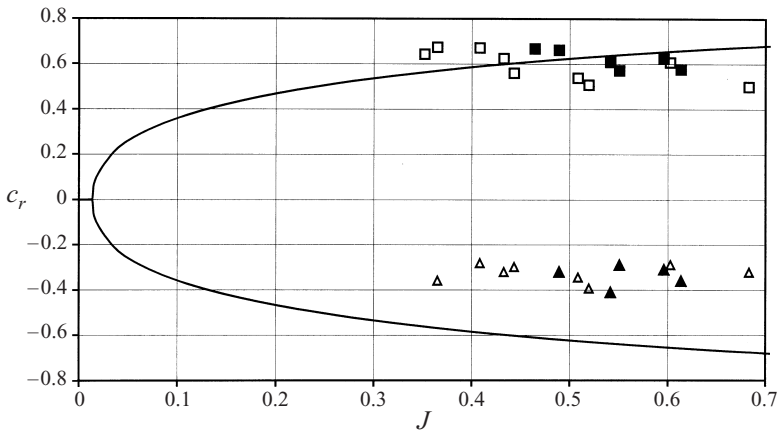


FIGURE 11. Comparison of measured wave speeds with predictions from Holmboe's analysis. The solid lines give the predicted wave speeds. Squares and triangles indicate measurements of positive and negative waves, respectively. Data from experiments 3 and 4 are indicated by solid and open symbols, respectively.

Lawrence, Haigh & Zhu (1998) show a significant effect when $R = 8$, $Re = 1200$ and continuous velocity and density profiles are assumed.

The good agreement between Holmboe's analysis and the experimental measurements of wavenumber (figure 10) may be due to the above modifications cancelling each other out. For instance for both positive and negative waves the effect of bounding the flow is to reduce the wavenumber at which the maximum growth rate occurs, whereas the effect of introducing viscosity, diffusivity and continuous profiles is to

https://doi.org/10.1017/S002211200000286X Published online by Cambridge University Press

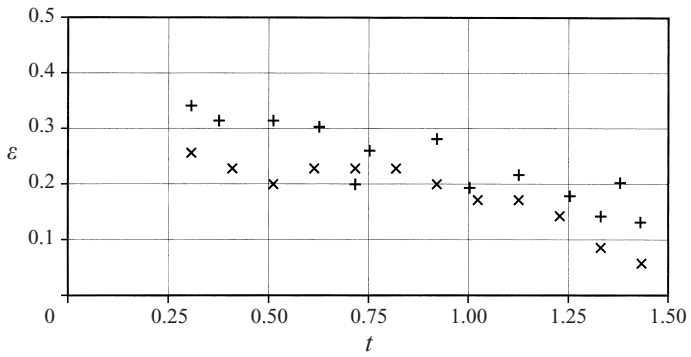


FIGURE 12. Comparison of the shift obtained using density and velocity profiles from experiment 3 with the shift predicted from $\varepsilon = c_r^+ + c_r^-$ (as in Eq. 3); ×, measurements; +, predictions.

increase this wavenumber. On the other hand modifications to Holmboe's analysis do not necessarily affect both positive and negative waves in the same manner. Non-zero values of ε have opposing effects on the wave speed of positive and negative waves, and this may partially explain the poor agreement between the predicted and measured negative wave speeds shown in figure 11.

Lawrence *et al.* (1991) showed that for piecewise-linear velocity and two-layer density profiles, the contour lines for c_r^+ and $\varepsilon - c_r^-$ coincide on stability diagrams. In other words the positive and negative waves move in opposite directions, but at the same speed with respect to the velocity at the level of the density interface. If this is in fact the case then the shift could be estimated from the wave speeds, using

$$\varepsilon = c_r^+ + c_r^-. \tag{3}$$

Estimates of ε for experiment 3 using (3) compare well with the measured values, given the level of experimental error involved, see figure 12. The flow configuration investigated by Lawrence *et al.* (1991) was quite idealized; whether (3) is of more general applicability, or not, is an interesting question for further investigation.

6. Concluding remarks

A laboratory study of the exchange of two fluids of different density through a constant-width channel containing an underwater sill has enabled us to study Holmboe's instability in greater detail than has been possible previously. The internal hydraulics of the exchange flow is such that we have been able to observe the initiation of instability, the behaviour of both symmetric and asymmetric Holmboe instabilities, and the suppression of the instability at high bulk Richardson numbers.

Various predictions of the conditions for instability have been verified. At the start of the experiment no instabilities appear, because the ratio R, of the vorticity thickness to the thickness of the density interface, is small. Similarly, if the exchange is driven by temperature differences rather than salinity differences, the low Prandtl number for heat ensures that R never increases beyond a critical value and instabilities never develop. Towards the end of the experiments the Richardson number increases beyond a critical value of approximately 0.7 and the flow stabilizes in accordance with the predictions of Nishida & Yoshida (1987). The Keulegan number is not an appropriate predictor of Holmboe's instability.

Predictions of the behaviour of the instabilities have also been tested. The wavenum-

https://doi.org/10.1017/S002211200000286X Published online by Cambridge University Press

bers of the instabilities all fall within the range predicted by Holmboe (1962) even though a number of his assumptions are violated. In general the negative waves do not travel as fast with respect to the mean flow as the positive waves. The wave speeds appear to be related to each other by the equation $\varepsilon = c_r^+ + c_r^-$, where ε is the vertical shift between the velocity and density interfaces. Changes in the wave speed of the negative waves occur as they pass through positive waves in accordance with nonlinear predictions; however, the positive waves do not appear to change speed. The above results suggest several possibilities for further numerical and experimental investigations of Holmboe's instability.

The authors would like to thank Drs Noboru Yonemitsu, Craig Steven, and Susan Haigh for their help during the various stages of this research, and Dr Bill Smyth for his insightful and helpful review. Financial support from the Natural Sciences and Engineering Research Council of Canada (NSERC) is gratefully acknowledged.

REFERENCES

Armi, L. & Farmer, D. M. 1988 The flow of Mediterranean water through the Strait of Gibraltar. *Prog. Oceanogr.* **21**, 1–105.

Bormans, M. & Garrett, C. 1989 The effects of non-rectangular cross section, friction, and barotropic fluctuations. *J. Phys. Oceanogr.* **19**, 1543–1557.

Breidenthal, R. 1981 Structure in turbulent mixing layers and wakes using a chemical reaction. *J. Fluid Mech.* **109**, 1–24.

Browand, F. K. & Wang, Y. H. 1972 An experiment on the growth of small disturbances at the interface between two streams of different densities and velocities. *Intl Symp. on Stratified Flows, Novosibirsk, USSR*, pp. 491–498. ASCE.

Browand, F. K. & Winant, C. D. 1973 Laboratory observations of shear-layer instability in a stratified fluid. *Boundary-Layer Met.* **5**, 67–77.

Dallimore, C. J., Imberger, J. & Ishikawa, I. 2000 Saline underflow into Lake Ogawara, *J. Hydraul. Engng ASCE* (submitted).

Grubert, J. P. 1989 Interfacial stability in stratified channel flows. *J. Hydraul. Engng* **115**, 1185–1203.

Haigh, S. P. 1995 Non-symmetric Holmboe waves. PhD thesis, Department of Mathematics, University of British Columbia.

Haigh, S. P. & Lawrence, G. A. 1999 Symmetric and nonsymmetric Holmboe instabilities in an inviscid flow. *Phys. Fluids* **11**, 1459–1468.

Hamblin, P. F. & Lawrence, G. A. 1990 Exchange flows between Hamilton Harbour and Lake Ontario. *Proc. 1990 Annual Conf. of Canadian Society for Civil Engineers*, vol. V; pp. 140–148.

Hazel, P. 1972 Numerical studies of the stability of inviscid stratified shear flows. *J. Fluid Mech.* **51**, 39–61.

Henderson, F. M. 1966 *Open Channel Flow*. MacMillan.

Holmboe, J. 1962 On the behaviour of symmetric waves in stratified shear layers. *Geofysiske Publikasjoner* **24**, 67–113.

Keulegan, G. H. 1949 Interfacial instability and mixing in stratified flows. *Res. Paper* RP 204. US Natl Bureau of Standards, vol. 43, pp. 487–500.

Koop, C. G. 1976 Instability and turbulence in a stratified shear layer. *Tech. Rep. USCAE* 134. Department of Aerospace Engineering, University of Southern California.

Koop, C. G. & Browand, F. K. 1979 Instability and turbulence in a stratified fluid with shear. *J. Fluid Mech.* **93**, 135–159.

Lawrence, G. A., Browand, F. K. & Redekopp, L. G. 1991 The stability of a sheared density interface. *Phys. Fluids* A **3**, 2360–2370.

Lawrence, G. A., Haigh, S. P. & Zhu, Z. 1998 In search of Holmboe instabilities. In *Physical Processes in Lakes and Oceans.* Coastal and Estuarine Studies, vol. 54 (ed. J. Imberger), pp. 295–304. AGU.

Moore, M. J. & Long, R. R. 1971 An experimental investigation of turbulent stratified shearing flow. *J. Fluid Mech.* **49**, 635–655.

https://doi.org/10.1017/S002211200000286X Published online by Cambridge University Press

Nishida, S. & Yoshida, S. 1987 Stability and eigen functions of disturbances in stratified two-layer shear flows. *Proc. Third Intl Symp. on Stratified Flows, Pasadena, California, 3–5 February 1987*, pp. 28–34.

Nishida, S. & Yoshida, S. 1990 Influence of the density and velocity profiles on calculated instability characteristics in an inviscid two-layer shear flow. *J. Hydrosci. Hydraul. Engng* **7**, 61–58.

Oguz, T., Ozsoy, E., Latif, M. A., Sur, H. I. & Unluata, U. 1990 Modeling of hydraulically controlled exchange flow in the Bosphorus Strait. *J. Phys Oceanogr.* **20**, 945–965.

Pouliquen, O., Chomaz, J. M. & Huerre, P. 1994 Propagating Holmboe waves at the interface between two immiscible fluid. *J. Fluid Mech.* **266**, 277–302.

Sargent, F. E. & Jirka, G. H. 1987 Experiments on saline wedge. *J. Hydraul. Engng* **113**, 1307–1324.

Scotti, R. S. & Corcos, G. M. 1972 An experiment on the stability of small disturbances in a stratified free shear layer. *J. Fluid Mech.* **52**, 499–528.

Smyth, W. D., Klaassen, G. P. & Peltier, W. R. 1988 Finite amplitude Holmboe waves. *Geophys. Astrophys. Fluid Dyn.* **43**, 181–222.

Smyth, W. D. & Peltier, W. R. 1989 The transition between Kelvin–Helmholtz and Holmboe instability; An investigation of the over reflection hypothesis. *J. Atmos. Sci.* **46**, 3698–3720.

Smyth, W. D. & Peltier, W. R. 1990 Three-dimensional primary instabilities of a stratified, dissipative, parallel flow. *Geophys. Astrophys. Fluid Dyn.* **52**, 249–261.

Smyth, W. D. & Peltier, W. R. 1991 Instability and transition in finite-amplitude Kelvin–Helmholtz and Holmboe waves. *J. Fluid Mech.* **228**, 387–415.

Stevens, C. L. & Coates, M. J. 1994 Application of a maximised cross correlation technique for resolving velocity fields in laboratory experiments. *J. Hydraul. Res.* **32**, 195–212.

Turner, J. S. 1973 *Buoyancy Effects in Fluids*. Cambridge University Press.

Yonemitsu, N. 1991 The stability and interfacial phenomena of a salt wedge flow. PhD thesis, Department of Civil Engineering, University of Alberta.

Yonemitsu, N., Swaters, G. E., Rajaratnam, N. & Lawrence, G. A. 1996 Shear instabilities in arrested salt-wedge flows. *Dyn. Atmos. Oceans* **24**, 173–182.

Yoshida S., Ohtani, M., Nishida, S. & Linden, P. F. 1998 Mixing processes in a highly stratified river. In *Physical Processes in Lakes and Oceans*. Coastal and Estuarine Studies, vol. 54 (ed. J. Imberger), pp. 389–400. AGU.

Zhu, D. Z. 1996 Exchange flow through a channel with an underwater sill. PhD thesis, Department of Civil Engineering, University of British Columbia.

Zhu, D. Z. & Lawrence, G. A. 2000 Hydraulics of exchange flows. *J. Hydraul. Engng* **126**, 921–928.

https://doi.org/10.1017/S002211200000286X Published online by Cambridge University Press